RSC Advances

ROYAL SOCIETY OF CHEMISTRY

www.rsc.org/advances

RSC Advances

ARTICLE

Valence-tautomeric infinite coordination polymer nanoparticles for encapsulation of Rhodamine B and its potential application for colorimetric and fluorescent dual mode sensing of hypochlorite

Received 00th January 20xx,
Accepted 00th January 20xx

DOI: 10.1039/x0xx00000x

www.rsc.org/

Xiaolei Zhang,[a] Jingjing Deng,[a]* Guoyue Shi[b] and Tianshu Zhou[a]*

In this work, we for the first time developed a visual and fluorescent dual probe for hypochlorite (ClO^-) based on stimuli-responsive valence-tautomeric infinite coordination polymer (ICP) nanoparticles encapsulated with a fluorescent dye, i.e., rhodamine B (RhB). In the absence of ClO^-, the as-formed RhB@{Co(3,5-dbsq)(3,5-dbcat)(bix)} ICP nanoparticles is well dispersed and quite stable in aqueous solution. However, the addition of ClO^- into the dispersion of RhB@{Co(3,5-dbsq)(3,5-dbcat)(bix)} destroys {Co(3,5-dbsq)(3,5-dbcat)(bix)} network structure, resulting in the release of RhB from ICP nanoparticles into the solvent. As a consequence, the color of the dispersion changed from purple to orange-red and, at the meantime, the fluorescence of RhB turns on, which constitutes a new mechanism for colorimetric and fluorescent dual-model sensing of ClO^-. With the method demonstrated here, the ClO^- in tap water can be easily visualized by the naked eyes and detected quantitatively through double channels. This study not only offers a new method for on-spot visible detection of ClO^- in environmental samples, but also provides a strategy for designing dual mode sensing mechanisms based on stimulus response of valence-tautomeric ICP nanomaterials.

Introduction

Nowadays, growing public concern has invigorated interest in detection and quantification of various contaminants in drinking water.[1,2] Hypochlorite (ClO^-) and its protonated form hypochlorous acid (HClO) can be easily encountered in our daily lives owing to its extensive applications such as drinking water disinfection, cooling water treatment and household bleaching, etc.[3,4] In water treatment, the concentration of free residual chlorine must be strictly controlled, because the low level cannot kill pathogenic bacteria and cause many hazards of an insufficient disinfection while the excessive intake and over-production of ClO^- can both elicit adverse health effects on human.[5-7] On the other hand, as one of the biologically important reactive oxygen species (ROS),[8-11] the excessive generation of ClO^- can cause many diseases including cardiovascular diseases, neuron degeneration, rheumatoid arthritis and even cancer.[12-15] Thus, development of a direct, sensitive, and selective method for hypochlorite residues in tap water is of great importance. Towards this end, several elegant methods have been developed for ClO^- determination, such as colorimetric, fluorescent, electrochemical and chromatographic methods and so forth.[16-24] However, the high requirements from on-spot practical applications for effective control of the drinking water quality, monitoring microbial population dynamics and understanding of the pathology of diseases substantially necessitate a new method for monitoring ClO^- both in method simplicity and sensitivity.[25,26]

Optical probes based on colorimetric and fluorescent responses are good candidates for realizing this goal. Because they not only enable the visualization of the target simply with bare eyes, but also validate a quantitative fluorescence assay in a simple and rapid feature.[27-30] However, most of the traditional probes for dual assay of ClO^- are prone to suffer the influence of the background fluorescence, solvent dependence and time-consuming synthesis.[31,32] So a novel material for ClO^- based on both color and fluorescence changes with excellent performance are still urgently needed. As a newly emerging fascinating nanomaterial, infinite coordination polymer (ICP) nanoparticles constructed from metal ions and organic bridging ligands, have activated growing interests because of their highly structural tailorability and excellent adaptive capability of guest encapsulation, which make them particularly attractive for dual-modal detection since the network and guest molecule could be rationally designed, respectively.[33-36] Herein, we employed a new strategy for the detection of ClO^- based on stimulus response of valence-tautomeric {Co(3,5-dbsq)(3,5-dbcat)(bix)} ICP nanoparticles encapsulated with RhB (RhB@{Co(3,5-dbsq)(3,5-dbcat)(bix)}) which could provide dual signal responses of both colorimetric and fluorescent outputs (Scheme 1).

[a] School of Ecological and Environmental Sciences, East China Normal University, 500 Dongchuan Road, Shanghai 200241, China. E-mail: tszhou@des.ecnu.edu.cn, jideng@des.ecnu.edu.cn Fax: +86-21-54341277, Tel: +86-21-54341277
[b] Department of Chemistry, East China Normal University, 500 Dongchuan Road, Shanghai 200241, China.Address here.
† Electronic Supplementary Information (ESI) available. See DOI: 10.1039/x0xx00000x

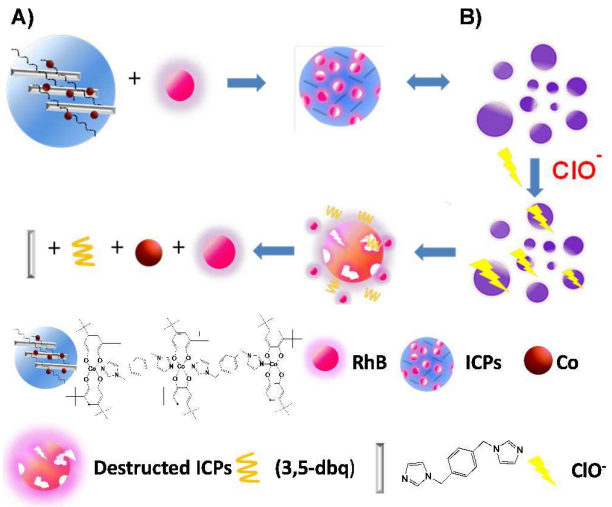

Scheme 1. A) Schematic illustration of the formation of RhB@{Co(3,5-dbsq)(3,5-dbcat)(bix)} ICP nanoparticles based on {Co(3,5-dbsq)(3,5-dbcat)} units through bix ligands with RhB entrapped. B) Schematic illustration of the colorimetric and fluorescent sensing of ClO^- based on the stimuli-responsive RhB@{Co(3,5-dbsq)(3,5-dbcat)(bix)} ICP nanoparticles with released RhB as the signal readout.

The valence-tautomeric ICP nanoparticles constructed with {Co(3,5-dbsq)(3,5-dbcat)} (3,5-dbsq$^-$ and 3,5-dbcat^{2-} are the semiquinonate radical and catecholate forms of 3,5-di-tert-butyl-1,2-benzoquinone (3,5-dbq), respectively) and bix (1,4-bis(imidazol-1-yl-methyl)benzene) ligand, in which fluorescent dye (i.e.,RhB) is used as a guest to form the RhB@{Co(3,5-dbsq)(3,5-dbcat)(bix)} ICP nanoparticles. By reversible intramolecular transfer involving the metal ion and the redox-active ligand, the network of {Co(3,5-dbsq)(3,5-dbcat)} interconvert reversibly between two valence tautomers—low-spin *ls*-[Co^{III}(3,5-dbsq)(3,5-dbcat)] and high-spin *hs*-[Co^{II}(3,5-dbsq)$_2$]. The network of {Co(3,5-dbsq)(3,5-dbcat)} ICP nanoparticles shows blue color, meantime, the trapped RhB shows magenta color. Accordingly, the RhB@{Co(3,5-dbsq)(3,5-dbcat)(bix)} ICP nanoparticles exhibit a purple color and weak emission of RhB in water. Upon the presence of ClO^-, the redox-active ligand 3,5-dbsq, 3,5-dbcat were oxidized to 3,5-dbq (yellow), resulting in the destruction of {Co(3,5-dbsq)(3,5-dbcat)(bix)} network and the release of encapsulated RhB into solution (Figure S1). As a result, RhB@{Co(3,5-dbsq)(3,5-dbcat)(bix)} ICP nanoparticles display the mixed color of 3,5-dbq and RhB (orange-red) and turn on the fluorescence of RhB, which provides a straightforward basis for the colorimetric and fluorescent dual assay for ClO^-. As we know, this is the first example of ClO^- detection based on stimuli-responsive ICP nanoparticles from colorimetric and fluorescent double signal. With the help of a UV-lamp (365 nm), this method can even possess on-site visible features in daytime and night easily, which could be further developed for simple environmental applications.

Experimental

Reagents and Materials.

α,α′-dichloro-p-xylene, 3,5-diterbutylbenzoquinone, 3,5-diterbutylcatechol were purchased from J&K. (Beijing, China). Cobalt acetate ($Co(CH_3COO)_2{\cdot}4H_2O$) was obtained from Aladdin Chemical Co. (Shanghai, China). Imidazole, sodium hydrogen phosphate, potassium dihydrogen phosphate, sodium hypochlorite, rhodamine B and potassium carbonate were from Sinopharm Chemical Reagent Co. (Shanghai, China). All chemicals were analytical grade reagents at least and used without further purification. All aqueous solutions were prepared with Milli-Q water (18.2 MΩ.cm) and all experiments were carried out at room temperature unless otherwise noted.

Synthesis of bix.

1,4-bis(imidazol-1-yl-methyl)benzene (bix) was synthesized as reported previously.[37] Briefly, a solution containing imidazole (3.16 g, 46.4 mmol) and α, α′-dichloro-p-xylene (0.78 g, 4.46 mmol) in methanol (50 mL) was refluxed for 18 h. Removal of methanol by evaporation gave a yellow syrup that was recrystallized from an aqueous solution of K_2CO_3 (6.13 g, 100 mL) to yield crystalline bix dehydrate.

Synthesis of {Co(3,5-dbsq)(3,5-dbcat)(bix)} particles and RhB@{Co(3,5-dbsq)(3,5-dbcat)(bix)} nanoparticles

{Co(3,5-dbsq)(3,5-dbcat)(bix)} ICP nanoparticles were synthesized with procedures reported previously.[38] The Co(3,5-dbsq)(3,5-dbcat)(bix) nanoparticles show adaptive encapsulation property towards some water-soluble dyes during the self-assembly process. Herein, RhB, was chosen as the guest molecular. Encapsulation of RhB into ICPs was performed by the following procedures. An aqueous solution of $Co(CH_3COO)_2{\cdot}4H_2O$ (120 mg, 0.5 mmol) was added to a ethanol solution (10 mL) of bix (121 mg, 0.5 mmol) and 3,5-diterbutylcatechol (110 mg, 0.5 mmol). Then 50 mL H_2O was added into the reaction mixture to produce a purple precipitatation consisting of RhB functionalized valence-tautomeric ICPs.

Colorimetric and fluorescent hypochlorite Sensing

The stock solutions of hypochlorite were prepared in PBS buffer solution (2 mM, pH 7.0) to cancel out the pH effect. RhB@{Co(3,5-dbsq)(3,5-dbcat)(bix)} ICP nanoparticles (0.8 mg) were dispersed into PBS buffer solution (2 mM, pH 7.0, 2000 μL) containing different concentrations of NaClO and the final concentrations of NaClO were 0 μM, 1 μM, 5 μM, 10 μM, 50 μM, 100 μM, 200 μM, 400 μM, 600 μM and 800 μM. After 3 min, the resulting mixtures were photographed in the ambient light and excited by a 365 nm UV-lamp in the dark respectively with a digital camera, and used UV-Vis spectrophotometer and fluorescence spectrophotometer for colorimetric and fluorescent detection, respectively.

Colorimetric and fluorescent sensing of hypochlorite in tap water.

The RhB@{Co(3,5-dbsq)(3,5-dbcat)(bix)} ICP nanoparticles (0.8 mg) dispersed in tap water (2000 μL) which containing

different concentrations of ClO^- (500 μM, 0 μL, 2 μL, 10 μL, 20 μL, 40 μL, 80 μL). The control group was prepared by adding RhB@{Co(3,5-dbsq)(3,5-dbcat)(bix)} ICP nanoparticles (0.8 mg) into Milli-Q water (2000 μL). The concentrations of ClO^- were determined through both UV-Vis and fluorescence spectrophotometer. Beyond that, the mixtures were photographed in ambient light and under UV-lamp respectively.

Results and discussion

Mechanistic Investigation on Colorimetric and Fluorescent Hypochlorite Assay

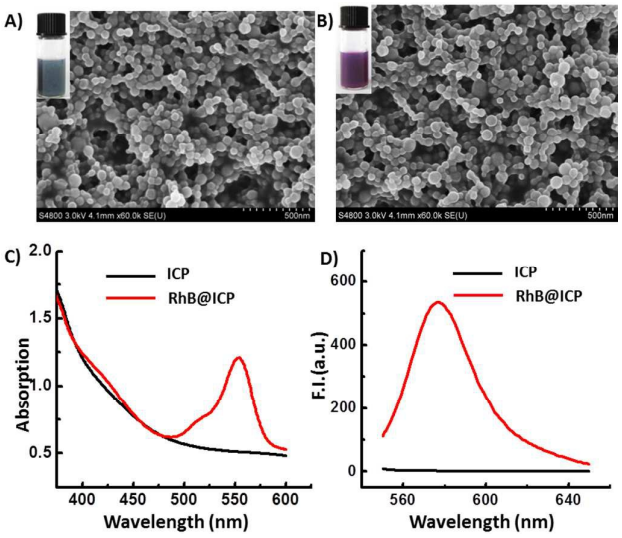

Figure 1. SEM image of {Co(3,5-dbsq)(3,5-dbcat)(bix)} ICP nanoparticles (A) and RhB@{Co(3,5-dbsq)(3,5-dbcat)(bix)} ICP nanoparticles (B) dispersed in Milli-Q water. Inset, photographs of the {Co(3,5-dbsq)(3,5-dbcat)(bix)} ICP nanoparticles (A) and RhB@{Co(3,5-dbsq)(3,5-dbcat)(bix)} ICP (B). C) UV-Vis spectra of the {Co(3,5-dbsq)(3,5-dbcat)(bix)} ICP nanoparticles (black curve) and RhB@{Co(3,5-dbsq)(3,5-dbcat)(bix)} (red curve) nanoparticles dispersed in PBS buffer solution. D) Fluorescent emission spectra of {Co(3,5-dbsq)(3,5-dbcat)(bix)} ICP nanoparticles (black curve) and RhB@{Co(3,5-dbsq)(3,5-dbcat)(bix)} nanoparticles (red curve) dispersed in PBS buffer.

The {Co(3,5-dbsq)(3,5-dbcat)(bix)} ICP nanoparticles were prepared by adding cobalt acetate aqueous solution into ethanol solution containing 3,5-dbcat and bix through self-assembly and the formed blue precipitation was characterized with scanning electron microscopy (SEM). SEM images of the resulting blue dispersion demonstrated the formation of spherical particles with the average size of 61.4±10.1 nm (Figure 1A). As shown in Figure 1B, the synthetic RhB@{Co(3,5-dbsq)(3,5-dbcat)(bix)} ICP nanoparticles have almost the same shape and size (diameter of 58.2±10.2 nm) as {Co(3,5-dbsq)(3,5-dbcat)(bix)} ICP particles, suggesting that the encapsulation of RhB does not change the morphology of {Co(3,5-dbsq)(3,5-dbcat)(bix)} network. However, the color of ICP nanoparticles changed from blue to purple (Figure 1B, inset), accompanying with the unique absorption peak of RhB at 554 nm in UV-Vis spectra (Figure 1C). When excited at 535 nm, the RhB functionalized ICP nanoparticles emits weak fluorescence at 578 nm (Figure 1D, red curve), thus may be ascribed to the suppression of {Co(3,5-dbsq)(3,5-dbcat)(bix)} ICP network (Figure 1D). These results demonstrated the successful formation of RhB@{Co(3,5-dbsq)(3,5-dbcat)(bix)} nanoparticles, which combined the inherent properties of both {Co(3,5-dbsq)(3,5-dbcat)(bix)} network and the trapped RhB.

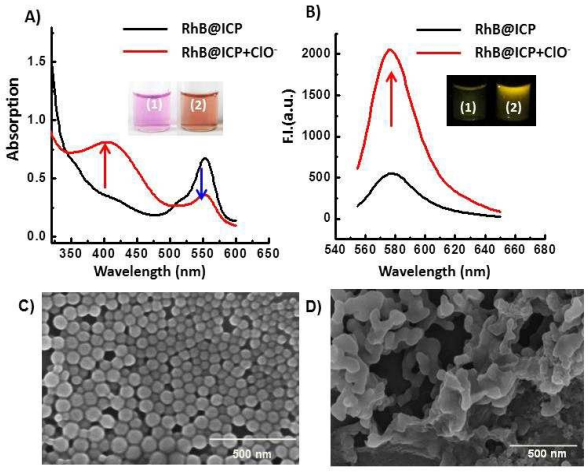

Figure 2. A) UV-Vis spectra of RhB@{Co(3,5-dbsq)(3,5-dbcat)(bix)} nanoparticles in PBS buffer without (black curve) and with (red curve) the presence of ClO^- (400 μM). Inset: Photographs of the dispersion without (vial 1) and with (vial 2) the addition of 400 μM ClO^-. B) Fluorescent emission spectra of RhB@{Co(3,5-dbsq)(3,5-dbcat)(bix)} nanoparticles dispersing in PBS buffer without (balck curve) and with (red curve) the addition of 400 μM ClO^- (λ_x=535 nm). Inset: Photographs of the dispersion without (vial 1) and with (vial 2) the addition of 400 μM ClO^- under 365 nm UV lamp. SEM image of RhB@{Co(3,5-dbsq)(3,5-dbcat)(bix)} ICP nanoparticles without (C) and with the addition of 400 μM ClO^- (D) dispersed in Milli-Q water.

As displayed in Figure 2A, the addition of ClO^- (80 μL, 4 mM) into PBS buffer containing RhB@{Co(3,5-dbsq)(3,5-dbcat)(bix)} ICP nanoparticles (0.8 mg) obviously lead to a color change of the dispersion from purple to orange-red, accompany with the production of a new absorbance peak at 411 nm (A_{411}) (red arrow), and the decrease of the absorbance peak of RhB at 554 nm (A_{554}) (blue arrow). Meanwhile, such a procedure also leads to a change in fluorescence channel. Upon the addition of ClO^-, the fluorescent spectrum shows an increase at 578 nm clearly (Figure 2B, red arrow). To further study the destruction of {Co(3,5-dbsq)(3,5-dbcat)(bix)}, the SEM images have been investigated. With the addition of ClO^-, the morphology of ICP nanoparticles changed from smooth spheres to irregular shape, some of the ICP nanoparticles aggregated and some of the particles collapsed (Figure 2C, D). This phenomenon could be due to the oxidation of ClO^- convert the redox-active ligand into 3,5-dbq, leading to the destruction of {Co(3,5-dbsq)(3,5-dbcat)(bix)} network and thereby the released RhB into the solution. The ratio of A_{411} to A_{554} (A_{411}/A_{554}) and fluorescent intensity of released RhB (I_{578}) could be considered as an

indicator for the degree of destruction of RhB@{Co(3,5-dbsq)(3,5-dbcat)(bix)} ICP nanoparticles caused by the oxidation of ClO^-. Thus, the colorimetric and fluorescence responding to ClO^- can be realized as demonstrated below. Here, we need to mention, to further investigate the decrease of the absorbance peak of RhB at 554 nm, transmittance (*T*) spectra of RhB@{Co(3,5-dbsq)(3,5-dbcat)(bix)} ICP nanoparticles were detected. As shown in Figure S2, the *T* of RhB@{Co(3,5-dbsq)(3,5-dbcat)(bix)} ICP nanoparticles at 554 nm increased. According to Lambert-Beer law, the absorbance spectrum of light absorption is defined as the logarithm of the ratio of the incident light intensity I_0 to the transmitted light intensity I_t, as shown formula 1. With the destruction of ICP nanoparticles upon addition of hypochlorite, the reflection of ICP nanoparticles decreased, thus increasing transmittance of RhB inside the blue shell (I_t, *T* of RhB entrapped increased). As a result, the A_{554} decreased.[39-44] Consequently, the ratio of the A_{411} to A_{554} was further developed as an indicator for the destruction of the RhB@{Co(3,5-dbsq)(3,5-dbcat)(bix)} ICP nanoparticles.

$$A = \lg(I_o/I_t) = \lg(1/T) \quad (1)$$

A: Absorbance I_o: Incident Light I_t: Transmission Light *T*: Transmittance

Sensitivity and Selectivity

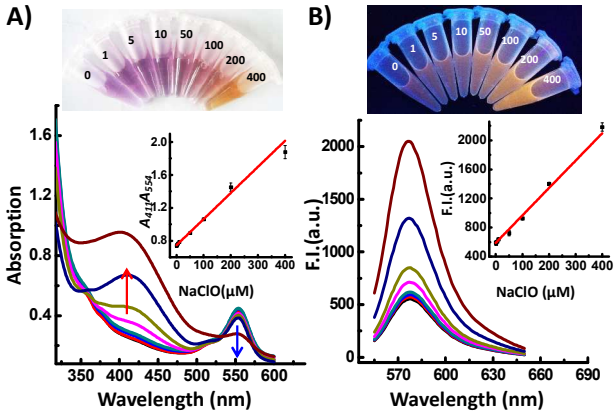

Figure 3. A) UV/Vis spectra and photographs (Upper) of RhB@{Co(3,5-dbsq)(3,5-dbcat)(bix)} nanoparticles in PBS buffer with the presence of different concentrations of ClO^-. Inset: Plot of A_{411}/A_{554} against ClO^- concentration. Each point was the average of three independent experiments. Error bars indicate standard deviations (n = 3). B) Fluorescence spectra and photographs (Upper) of RhB@{Co(3,5-dbsq)(3,5-dbcat)(bix)} nanoparticles in PBS buffer with the presence of different concentrations of ClO^-. Inset: I_{578} as a function of the concentration of hypochlorite ions when excited at 535nm.

To optimize the conditions before detection, we considered the pH range and the time course of the fluorescence response of this dual probe upon addition of ClO^-. As demonstrated in Figure S3 A, B, the RhB@{Co(3,5-dbsq)(3,5-dbcat)(bix)} nanoparticles in PBS buffer with different pH valve from 7.0 to 8.5 did not result in an obvious change in the fluorescent intensity and different concentration of hypochlorite induced the slight pH change in PBS buffer, which did not affect our measurement. Figure S3 C, D, shows that the fluorescent spectra increased gradually with the reaction time until 100 s. To make sure the reaction adequately, 3 min was chosen as the optimized reaction time in the sequent experiment.

Under the optimal conditions, the sensitivity of the colorimetric and fluorescent sensing of ClO^- was evaluated as depicted in Figure 3 and S4. The addition of various concentrations of ClO^- to the dispersion gradually turns the color from purple to orange-red in ambient light, accompanying with a dramatic change in the UV-Vis spectra of the dispersion; with increasing the concentration of ClO^-, A_{411} increases, while A_{554} decreases. The ratio of A_{411}/A_{554} increases within a concentration range from 1 μM to 400 μM (A_{411}/A_{554} = 0.404+0.00347 C/μM, R^2 = 0.998) (Figure 3A). Meanwhile, the addition of ClO^- also leads to increase of fluorescent intensity at 578 nm, which shows a linear response range from 1 μM to 400 μM (I=552.191+3.704 C/μM, R^2=0.995) (Figure 3B). Since our colorimetric channel was ratiometric, thus high sensitivity could be achieved by the amplified signal readout through simultaneous readings of two wavelengths. As a result, the working concentration range of double channel was almost the same.[27] The basal level of ClO^- in environmental systems is on the micromolar scale which just falls within the linear range of the present analytical method,[40-43] thus confirming that the strategy developed in this study is able to realize the dual channel detection of ClO^- in aquatic environment.

By using ClO^- as the oxidant, we next studied the selectivity of this double signal-based method. Various environmentally relevant ions and oxidants were taken into account.[49] As illustrated in Figure 4, the separate addition of each kind of anion (200 μL, 2 mM) including SO_4^{2-}, Ac^-, CO_3^{2-}, NO_2^-, NO_3^-, I^-, NH_4^+, Cl^-, Ca^{2+} and Mg^{2+} into the dispersion of PBS buffer containing RhB@{Co(3,5-dbsq)(3,5-dbcat)(bix)} nanoparticles (0.8 mg, 1800 μL) did not result in an obvious change either in the color (Figure 4A) or in the fluorescent intensity (Figure 4B), however, the addition of ClO^- (200 μL, 2 mM) induced an obvious color change (from purple to orange-red) and a significant enhancement of fluorescent intensity of the dispersion. To further explore the selectivity of this colorimetric and fluorescent method toward ClO^-, the absorption ratio of A_{411}/A_{554} and the fluorescent intensity of the dispersion were shown by the red bar in Figure 4C and 4D. These results substantially demonstrate the present method has a high selectivity against these potential interferences in environmental water. This property, along with the good linearity, substantially enables the utilization of the stimuli-responsive RhB@{Co(3,5-dbsq)(3,5-dbcat)(bix)} ICP nanoparticles for ClO^- detection, and essentially offers a technically simple yet rapid approach to direct sensing of ClO^- in tap water.

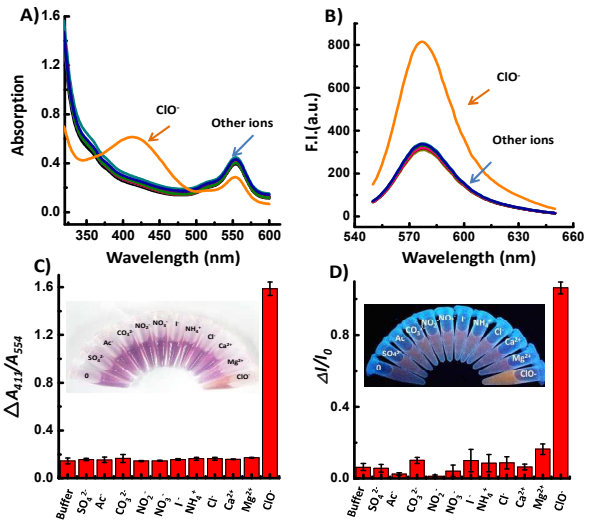

Figure 4. UV-Vis spectra (A) and fluorescence spectra (B) of RhB@{Co(3,5-dbsq)(3,5-dbcat)(bix)} ICP nanoparticles in PBS buffer with the presence of various relevant ions at a concentration of 200 μM. C) Values of △A411/A554 obtained from UV-Vis spectra and photographs (inset) of RhB@{Co(3,5-dbsq)(3,5-dbcat)(bix)} ICP nanoparticles dispersion responses to various ions. Error bars show the standard deviations (n = 3). D) Values of △I/I0 obtained from fluorescence spectra and photographs (inset) of RhB@{Co(3,5-dbsq)(3,5-dbcat)(bix)} ICP nanoparticles dispersion responses to various ions when excited by a 365nm UV lamp. Error bars show the standard deviations (n = 3).

Colorimetric and Fluorescent Sensing of ClO⁻ in Tap water

To demonstrate the validity of our colorimetric and fluorescent method for sensing of ClO^- in tap water, we applied a standard addition method to compensate matrix effects and obtained stability and accuracy also.[50] RhB@{Co(3,5-dbsq)(3,5-dbcat)(bix)} ICP nanoparticles were first dispersed in tap water, and then different amounts of ClO^- were spiked into the tap water to estimate the ClO^- level in the sample. As a comparison, the RhB@{Co(3,5-dbsq)(3,5-dbcat)(bix)} ICP nanoparticles were also dispersed in Milli-Q water (without ClO^- as control). The results are shown in Figure 5, where the ClO- in tap water could be determined both by color change (from purple to orange-red, Figure 5A, inset) and the enhancement of fluorescent intensity (Fig. 5B, inset) with the help of a 365 nm UV lamp by naked eyes. Moreover, It was found that the ratio of A_{411}/A_{554} from UV-Vis spectra provides a linear response to ClO^- spiked into tap water and the regression equation is A_{411}/A_{554} = 0.20599 + 0.00401 C/μM, R^2= 0.997 (Figure 5C). Similarly, the fluorescent intensity at 578 nm from fluorescent spectra also shows a linear response towards ClO^- spiked into tap water and the regression equation is I = 118. 36025 + 2.32278 C/μM, with R^2= 0.993 (Figure 5D).By using the standard addition method mentioned above, we estimated that the concentration of ClO^- in the tap water is 51.4 μM and 50.9 μM by colorimetric channel and fluorescent channel, respectively, which showed great consistency with each other (Figure 5C,D) and data reported previously.[51] These properties validate the reliability of this colorimetric and fluorescent method based on stimuli-responsive RhB@{Co(3,5-dbsq)(3,5-dbcat)(bix)} ICP nanoparticles in real sample detection.

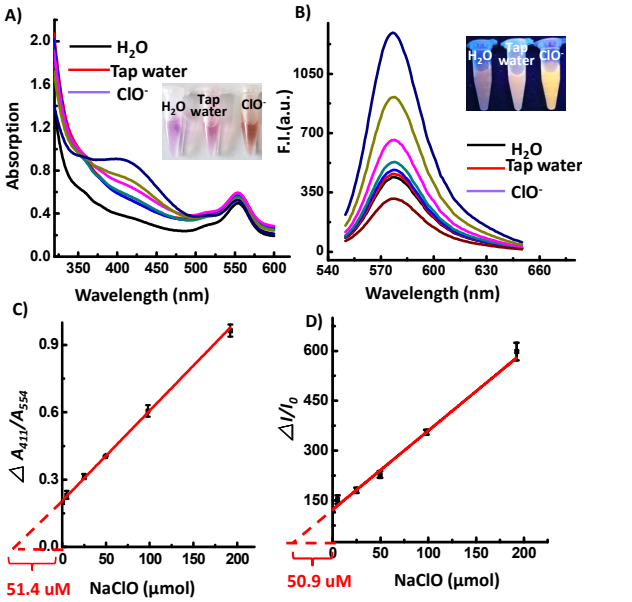

Figure 5. UV-Vis spectra of RhB@{Co(3,5-dbsq)(3,5-dbcat)(bix)} ICP nanoparticles in Milli-Q water (vial 1, black curve), tap water (vial 2, red curve), tap water spiked with ClO^-, respectively. Inset: Photographs of RhB@{Co(3,5-dbsq)(3,5-dbcat)(bix)} ICP nanoparticles in Milli-Q water (black curve), tap water (red curve), tap water spiked with ClO^- (violet curve). B) Fluorescence spectra of the dispersion in Milli-Q water (black curve), tap water (red curve), tap water spiked with ClO^-, respectively. Inset: Photographs of the dispersion in the Milli-Q water (vial 1, black curve), tap water (vial 2, red curve), tap water spiked with ClO- (violet curve) when excited by a 365 nm UV lamp. C) Plot of $\triangle A_{411}/A_{554}$ (A_{411}/A_{554} (tap water) - A_{411}/A_{554} (Milli-Q water)) against the ClO^- concentration. Error bars show the standard deviations (n = 3). D) Plot of $\triangle I$ (I_{578} (tap water)-I_{578}(Milli-Q water)) against the ClO^- concentration. Error bars show the standard deviations (n = 3).

Conclusions

On the basis of the stimulus-response of valence-tautomeric RhB@{Co(3,5-dbsq)(3,5-dbcat)(bix)} ICP nanoparticles, we have for the first time demonstrated a simple and yet effective colorimetric and fluorescent dual probe for ClO^-. The dual signal response and excellent analytical properties of this method validate it is a reliable approach for accurate determination of ClO^- in tap water, and this method could be further developed as test paper for on-site ClO^- detection, which is of great importance in drinking water safety. Moreover, this colorimetric and fluorescent dual system offers a new strategy and great promise for other pollutant molecules detection by rational designing the nanostructures of novel infinite coordination polymer nanoparticles.

Acknowledgements

This work is supported by the National Natural Science Foundation of China (No. 21277048, 21505046).

Notes and references

1 Richardson, S. D.; Ternes, T. A. *Anal. Chem*. 2014, **86**, 2813-2848.
2 Zhu, J.; Liu, S.; Liu, Z.; Li, Y.; Qiao, M.; Hu, X. *RSC Adv*. 2014, **4**, 5990-5994.
3 Chen, W.; Venkatesan, P.; Wu, S. *Anal. Chim. Acta* 2015, **882,** 68–75.
4 Xia, X.; Zhang, Y.; Wang, J. *RSC Adv*. 2014, **4**, 25365-25368.
5 Li, J.; Hou, F.; Yin, C. *RSC Adv*. 2014, **4**, 44610-44613.
6 Dong, Y.; Li, G.; Zhou, N.; Wang, R.; Chi, Y.; Chen, G. *Anal. Chem.* 2012, **84**, 8378-8382.
7 Zhang, J.; Yang, X. *Analyst* 2013, **138**, 434-437.
8 Chen, S.; Lu, J.; Sun, C.; Ma, H. *Analyst* 2010, **135**, 577.
9 Reja, S.; Bhalla, V.; Sharma, A.; Kaur, G.; Kumar, M. *Chem. Commun.* 2014, **50**, 11911-11914.
10 Sokolovskaya, E.; Rahmani, S.; Misra, A. C.; Brase, S.; Lahann, J. ACS *Appl. Mater. Interfaces* 2015, **7**, 9744–9751.
11 Qin, L. W.; Ma, D.; Li, D. W.; Li, Y.; Chen, H. B.; Kraatz, T. D.; James, Y. T. *Chem. Eur. J.* 2011, **17**, 5262-5270.
12 Yang, Y.; Lu, H.; Wang, W.; Liau, I. *Anal. Chem*. 2011, **83**, 8267-8272.
13 Steinbeck, M. J.; Nesti, L. J.; Sharkey, P. F.; Parvizi, J. J. *Orthop. Res*. 2007, **25**, 1128-1135.
14 Huo, F. J.; Zhang, J. J.; Yang, Y. T.; Chao, J. B.; Yin, C. X.; Zhang, Y. B.; Chen, T.G. Sensors and Actuators B 2012, **166**, 44-49.
15 Li, J.; Huo, F.; Yin, C. RSC Adv. 2014, **4**, 44610-44613.
16 Zhang, J.; Wang, X.; Yang, X. *Analyst* 2012, **137**, 2806-2812.
17 Chen, X.; Tian, X.; Shin, I.; Yoon, J. *Chem. Soc. Rev.* 2011, **40**, 4783-4804.
18 Sun, M.; Yu, Huan.; Zhu, H.; Ma, F.; Zhang, S.; Huang, D.; Wang, S. *Anal. Chem.* 2014, **86**, 671-677.
19 Hou, J.; Wu, M.; Li, K.; Yang, J.; Yu, K.; Xie, Y.; Yu, X. *Chem. Commun*. 2014, **50**, 8640.
20 Su, W.; Tian, Y.; Peng, S. *Appl. Surf. Sci.* 2014, **315**, 95-103.
21 Gallina, A.; Pastore, P.; Magno, F. *Analyst* 1999, **124**, 1439-1442.
22 Yang, Y.; Yin, C.; Huo, F.; Chao, J.; Zhang, Y.; Jin, S. Sensors and Actuators B 2014, **199**, 226-231.
23 Xu, Q.; Lee, K. A.; Lee, S.; Lee, M. K.; Lee, W. J.; Yoon, J. *J. Am. Chem. Soc*. 2013, **135**, 9944−9949.
24 Xu, Q.; Heo, C. H.; Kim, G.; Lee, H. W.; Kim, H. M.; Yoon, J.; *Angew.Chem.* 2015, **127**, 4972 –4976.
25 Shyamaprosad, G.; Avijit, K. D.; Abhishek, M.; Anup, K. M.; Partha, S.; Ching, K. Q.; Fun, H. K.; Hatem, A. *Anal.Chem.* 2014, **86**, 6315-6322.
26 Yao, Z.; Ma, W.; Yang, Y.; Chen, X.; Zhang, L.; Lin, C.; Wu, H. C. *Org. Biomol. Chem.* 2013, **11**, 6466-6469.
27 Deng, J.; Yu, P.; Wang, Y.; Mao, L. *Anal. Chem*. 2015, **87**, 3080-3086.
28 Yao, Z.; Bai, H.; Li, C.; Shi, G. *Chem. Commun*. 2011, **47**, 7431-7433.
29 Tan, D.; He, X.; Xing, X.; Zhao, Y.; Tang, H.; Pang, D. *Talanta* 2013, **113**, 26-30.
30 Kumar, V. V.; Anthony, S. P. *RSC Adv*. 2014, **4**, 18467-18472.
31 Li, C.; Zhou, Y.; Li, Y.; Kong, X.; Zou, C. *Anal. Chim*. Acta. 2013, **774**, 79-84.
32 Zha, J.; Fu, B.; Qin, C.; Zeng, L.; Hu, X. *RSC Adv*. 2014, **4**, 43110-43113.
33 Imaz, I.; Maspoch, D.; Rodrguez, C. B.; Prez, F. J. M.; Campo, J.; Ruiz, D. M. *Angew. Chem., Int. Ed.* 2008, **47**, 1857-1860.
34 Sato, O.; Cui, A.; Matsuda, R.; Tao, J.; Hayami, S. *Acc. Chem. Res*. 2007, **40**, 361-369.
35 Imaz, I.; Marta, R. M.; Lorena, G. F.; Francisca G.; Daniel, R. M.; Jordi H.; Victor, P.; Daniel, M. *Chem. Commun*. 2010, **46**, 4737-4739.
36 Tan, H.; Li, Q.; Zhou, Z.; Ma, C.; Song, Y.; Xu, F.; Wang, L. *Anal. Chim*. Acta. 2015, **856**, 90-95.
37 Hoskins, B. F.; Robson, R.; Slizys, D. A. J. *Am. Chem. Soc*. 1997, **119**, 2952-2953.
38 Imaz, I.; Hernando, J.; Ruiz, M. D.; Maspoch, D. *Angew. Chem., Int. Ed.* 2009, **48**, 2325-2329.
39 Roy, I.; Ohulchanskyy, T. Y. ; Pudavar, H. E.; Bergey, E. J.; Oseroff, A. R.; Morgan, J.; Dougherty, T. J.; Prasad, P. N. J. *Am. Chem. Soc.* 2003, **125**, 7860-7865.
40 Deng, J.; Ma, W.; Yu, P.; Mao. L. *Anal. Chem*. 2015, **87**, 6958-6965.
41 Dwivedi, C.; Chaudhary, A.; Gupta, A.; NandiJi, C. K. ACS *Appl. Mater. Interfaces* 2015, **7**, 5039−5044.
42 Niu, H.; Wang, S.; Zhou, Z.; Ma, Y.; Ma, X.; Cai, Y. *Anal. Chem*. 2014, **86**, 4170-4177.
43 Greathouse, J. A.; Allendorf, M. D. J. *Am. Chem. Soc.* 2006, **128**, 10678-10679.
44 Yuan, Y.; Min, Y.; Hu, Q.; Xing, B.; Liu, B. *Nanoscale* 2014, **6**, 11259-11272.
45 Standardization Administration of the People's Republic of China (SAC) has set the drinking water sanitary standard (GB5749-2006).
46 Standardization Administration of the People's Republic of China (SAC) has set the surface water environment quality standard (GB3838-2002).
47 Standardization Administration of the People's Republic of China (SAC) has set the hospital sewage discharge standard (GBJ48-83).
48 Kong, B.; Zhu, A.; Luo, Y.; Tian, Y.; Yu, Y.; Shi, G. *Angew. Chem., Int. Ed.* 2011, **50**, 1837-1840.
49 Yu, Q.; Zhang, Y. K.; Liang, H.; Zhao, Q.; Yang, T.; Liu, S.; Zhang, C.; Shi, Z.; Xu, W.; Huang, W. ACS *Appl. Mater. Interfaces* 2015, **7**, 5462–5470.
50 Masoud, S. R.; Mohsen, I.; Niloufar, A.; Mojtaba; S. *Chemometr. Intell. Lab*. 2013, **120**, 77-83.
51 Lou, X.; Zhang, Y.; Li, Q.; Qin, J.; Li, Z. *Chem. Commun*. 2011, **47**, 3189-3191.

Table of Contents:

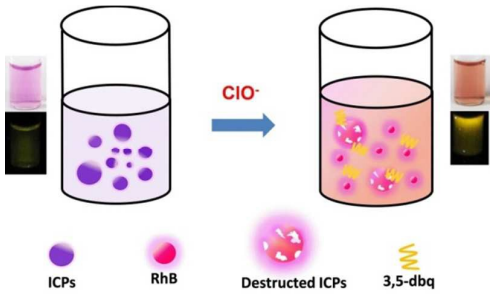

The colorimetric and fluorescent ClO^- sensing based on the stimulus response of valence-tautomeric RhB@{Co(3,5-dbsq)(3,5-dbcat)(bix)} ICP nanoparticles.

Highlights:

- Valence-tautomeric RhB@{Co(3,5-dbsq)(3,5-dbcat)(bix)} ICP nanoparticles were synthesized as colorimetric and fluorescent dual probe.
- This dual probe shows high selectivity and sensitivity for ClO^- assay.
- This dual probe could be applied for monitoring ClO^- in tap water directly.
- This method offered a new strategy for other contaminants detection based on novel ICP nanoparticles.